The Cryogenic Anticoincidence Detector for ATHENA-XMS

C. Macculi · L. Colasanti · S. Lotti · L. Natalucci · L. Piro · D. Bagliani · M. Biasotti · F. Gatti · G. Torrioli · M. Barbera · G. La Rosa · T. Mineo · E. Perinati

Abstract The TES cryogenic detectors, due to their high spectral resolution and imaging capability in the soft X-ray domain, are the reference devices for the next proposed space missions whose aims are to characterize the spectra of faint or diffuse sources. ATHENA is the re-scoped IXO mission, and one of its focal plane instrument is the X-ray Microcalorimeter Spectrometer (XMS) working in the energy range 0.3–10 keV. XMS will be able to achieve the proposed scientific goals if a background lower than 0.02 cts/cm^2/s/keV is guaranteed. The studies performed by GEANT4 simulations depict a scenario where it is mandatory to use an active Anti-Coincidence (AC) to reduce the expected background in the L2 orbit down to the required level. This is possible using a cryogenic AC detector able to provide a rejection efficiency of about 99%. We are developing for this purpose a TES-based detector made by Silicon absorbers (total assembled area about 1 cm^2 and 300 μm thick) and sensed by a Ir:Au TES. All the work done for IXO is applicable to ATHENA, with more margins

C. Macculi (✉) · L. Colasanti · S. Lotti · L. Natalucci · L. Piro
INAF/IASF Roma, Via del Fosso del Cavaliere, 100, 00133 Roma, Italy
e-mail: claudio.macculi@iasf-roma.inaf.it

L. Piro
Astronomy Department, Faculty of Science, King Abdulaziz University, P.O. Box 80203, Jeddah 21589, Saudi Arabia

D. Bagliani · M. Biasotti · F. Gatti
Phys. Dep., Genova University, Via Dodecaneso 33, 16146 Genova, Italy

G. Torrioli
CNR/IFN, Via Cineto Romano, 42, 00156 Roma, Italy

M. Barbera
Phys. Dep., Palermo University, Via Archirafi 36 I, 90123 Palermo, Italy

G. La Rosa · T. Mineo · E. Perinati
INAF-IASF Palermo, Via Ugo La Malfa 153, 90146 Palermo, Italy

due to the smaller area required for the detector. Here we present the results obtained from different samples, as a step towards the final detector design.

Keywords Low temperature detectors · Astronomy and astrophysics · Superconductivity · Silicon · TES

1 Introduction

A cryogenic anticoincidence detector has already successfully flown on board the SUZAKU mission: it is a LVSID (Low Voltage Silicon Ionizing Detector) [1] type sensor. The implementation of a TES-based detector as anticoincidence for a TES calorimeters array offers several advantages compared to LVSID, including a faster response and easier mechanical, electrical and thermal interfaces with a TES-based main array. A LVSID-based anticoincidence has been employed with the Suzaku XRS microcalorimeter, and it fits well with such a sensor, employing the same typology of JFET-based pre-amplifiers, operated around 120 K. On the contrary for XMS the front-end electronics of the array is based on SQUID, the same employed by a TES-based anticoincidence, both operated at much lower temperature. In addition, the TES array delivers faster signals, thus requiring a faster anticoincidence veto signal. Motivated by these advantages, we have base-lined for XMS a TES-based anticoincidence. We have first characterized the scaling from small size to the final detector, with 1 cm^2 area^2. A key element is the understanding of the physics of the detector, where key processes include quasiparticle recombination, and two different regimes related to thermal and a-thermal phonons are present (for a review see [3]). We remark that the absorber is made of Silicon, and the TES is an Ir:Au bilayer. Due to the semiconductor absorber about 70% of the primary energy goes into phonons. The remaining 30% is lost since it is shared by electron-hole pairs [4, 5]. The a-thermal signal can provide a fast flag to reject the particle background, by keeping under control the SQUID slew rate. A short list of the requirements are reported in the following Table 1.

Our consortium has developed a series of prototypes, and here we present a more detailed and updated analysis of the one shown in [2]. The results confirm the design for IXO/ATHENA cryogenic anticoincidence detectors and improve its TRL [6] (Technology Readiness Level). Here we report only the results related to the parameters that help us in understanding the physical scenario. The reference models are: AC-S1, AC-S2 and AC-S3. Most of the physical and geometrical information are in [2, 6]. The detectors are not been operated in extreme ETF (Electro-Thermal Feedback) since $T_b \sim T_C$. Usually the loop gain $L_{ETF} \sim 2$. Further on, we note that the AC-S2 and AC-S3 detectors, originally dimensioned for the IXO

Table 1 ATHENA CryoAC requirements (short list)

Rise Time constant	<30 μs
Time constant Decay	<300 μs (Goal)
Bandpass	20 keV–0.5 MeV
Total Area	~1 cm^2

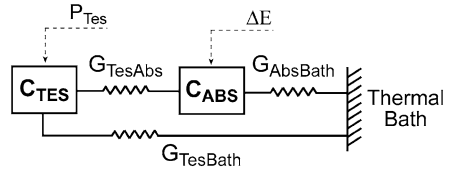**Fig. 1** Thermal design of the detectors. "$G_{TesBath}$" is the usual bonding

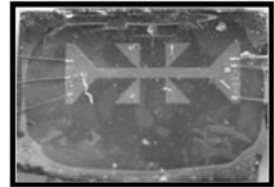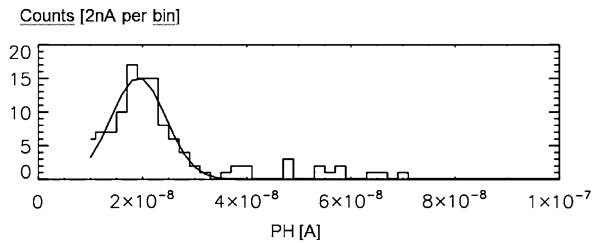
Fig. 2 The AC-S1 detector

Fig. 3 ^{55}Fe AC-S1 acquired spectrum. The threshold is ~10 nA

array, have an area which is now 4 times larger than required by the ATHENA CryoAC.

Finally, we remark the thermal design [7] of the microcalorimeters here analysed that are different with respect to the usual one, as shown in Fig. 1.

2 AC-S1: Analysis and Results

The detector (see Fig. 2) has a Si absorber with area of 16.5 mm^2, a thickness of 300 um and a TES with an area of 3.7 mm^2. With respect to the ATHENA configuration, based on a 4 pixel CryoAC design as for IXO, its area is just a factor 1.5 lower.

The detector has been operated with a mixed thermal/ a-thermal regime, and the acquired spectrum is shown in Fig. 3.

The pulse analysis has been based on the spectrum in order to understand if the pulse shape depends also on its amplitude. We have divided the spectrum in zones (multiple of the noise rms around the peak where $\sigma_i \sim 2$ nA), and analyzed the pulses in each of one (more detail in [7]).

Figure 4 shows the average pulse in a section around the peak: it is composed by the thermal (slow) component plus the athermal (fast) one. As shown, the pulse is quite fast in rising, a phase indeed dominated by the a-thermal component. The average rise time constant is $\tau_R \sim 1$ μs (see [2]). Results of data fitting with double pulse, in terms of residuals with respect to the data are shown in Fig. 4 [7, 8].
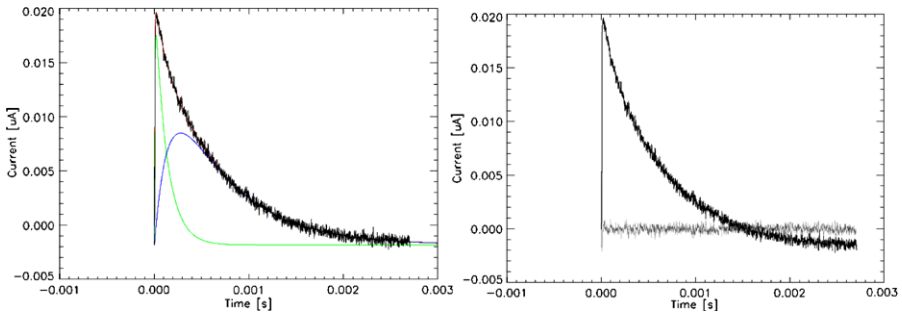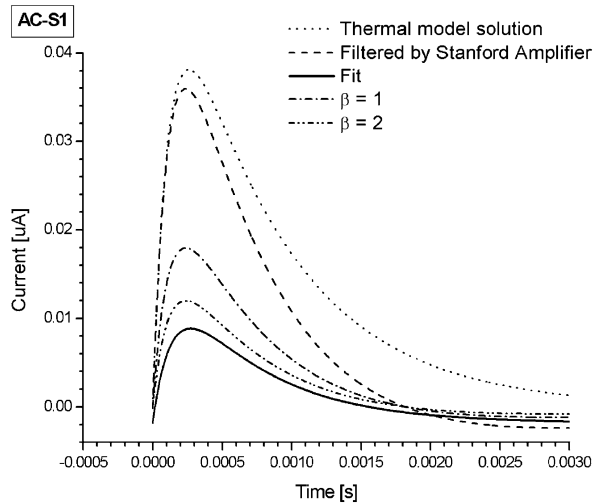
Fig. 4 (Color online) (*Left*) Average 6 keV-pulse fitted by a double component: Athermal (the fast one) and Thermal (the slow one). (*Right*) The residuals: double pulse component fit

Fig. 5 Expected thermal component scenario. The "Fit" curve is the expected thermal trend as evaluated from the data

The model shown in Fig. 1 which sets the thermal component has been implemented and both the numerical and analytical solutions about the expected TES pulse compared: they are fully consistent [7].

It has been converted in current and also filtered since the acquired pulses have been worked by the Stanford amplifier (model SR560) [6]. So, the resulted pulse has been compared with the thermal component coming from the double-pulse fitting procedure. The result is in Fig. 5.

There is a good agreement, in terms of amplitude and rise/decay times, if it is also taken into account that all the thermal parameters has been evaluated and not measured. Unfortunately an evaluation of the β parameter (i.e. the current sensitivity) is not available, and typical values have been adopted.

The presence of a double component is also statistically confirmed by the F-test, performed by comparing the double-pulse fit test results with respect to the single-pulse test (reduced chi-square for both is ∼1). At 99% of CL, the critical value for F is $F_{0.01,3,\infty} = 3.78$. From the data we have obtained $F > 100$. Further on, the rise time of the a-thermal pulse is essentially determined by the propagation of phonons,

Table 2 Updated AC-S1 main results. The collecting area is TES area-to-absorber area ratio

Collecting area (%)	τ_R [μs]	τ_D [μs]	Threshold [keV]	E_{max} [keV]
11	<1	~600	3	460

and the coupling between the Si and TES is no more described by the usual conductance in thermal equilibrium. We therefore take, as reference, rise time values observed from experiments [9, 10], which are typically of the order or shorter than 1 μs. The decay of the a-thermal pulse can be derived in a simplified scenario as follows. After being heated by the a-thermal phonons, the electron gas of the TES release the heat towards the Si absorbers as a thermal process characterized by the coupling between Si and TES. Therefore we expect a decay time of the a-thermal component similar to the rise time of the thermal pulse. This is clearly shown in Fig. 4-left.

By taking into account both the conversion from the input energy (~6 keV, ^{55}Fe) to the measured energy and aspects related to the working point, the threshold for this detector is ~3 keV and the expected time constant decay is consistent with the value expected for the thermal component [2, 6], whose amplitude is depleted due to both the high thermal coupling to the bath ($G_{AbsBath} = 12$ nW/K) which is close to the coupling between the absorber and the TES ($G_{TesAbs} = 8.6$ nW/K) and the TES heat capacity (14 pJ) which is greater than the absorber one (2.5 pJ) [3, 7].

Finally, the pulse grows as athermal and decays as thermal one.

The updated AC-S1 main results are summarized in Table 2. It is noteworthy that the E_{max} (i.e. the energy range) parameter has been evaluated by the R-T TES transition curve. It means that if sufficient thermal damping is guaranteed, the energy of the incident primary particle, less than E_{max}, is converted in an athermal detectable signal which is inside the TES functional range. We remark the presence of the athermals by the F-test.

3 AC-S2: Analysis and Results

A larger area prototype (100 mm^2), AC-S2 employs 4 TESes (1.5 mm^2 each), each in contact with a couple of Al pads (1.5 mm^2 each; see also [1], operated in parallel readout configuration. The Al pads increase the effective collecting area since the quasi-particles produced by high energy phonons diffuse towards the TES giving an additional heat signal. The detector has been illuminated by the ^{241}Am shielded source (only 60 keV line). In Fig. 6 below are shown both the detector picture and the spectrum.

The spectrum is obtained from the events which exceed their $5 \cdot \sigma_V$ threshold (the average rms noise of the baselines is ~0.009 V). It is not symmetric. The threshold is about 40 keV. Figures 7, 8, 9 show that the pulses are quite fast. In particular, the Rise time constant is compatible with the expected value due to the L/R cutoff (~1 μs). It is noteworthy that only one pulse family is evident, and it
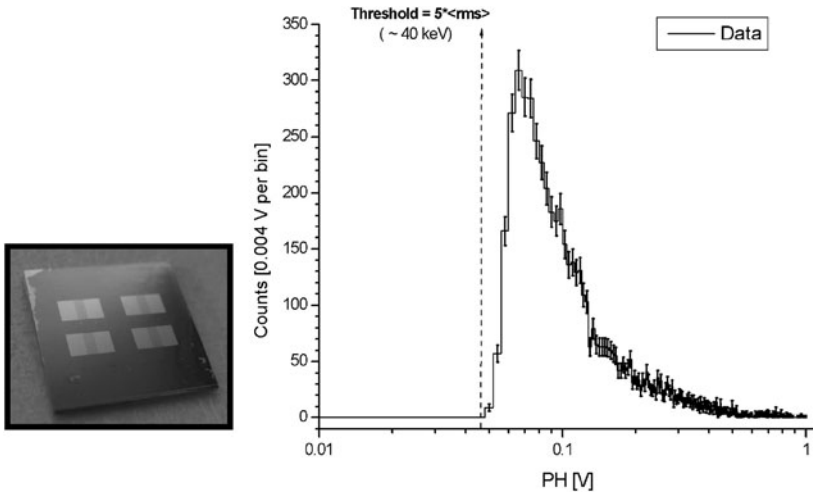
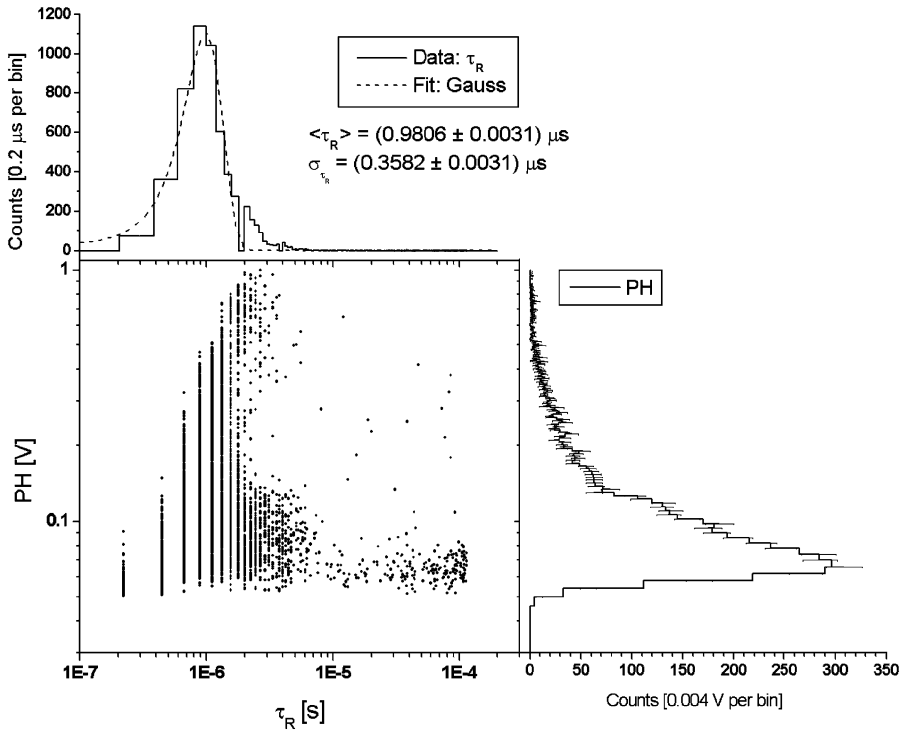**Fig. 6** (*Left*) The detector. (*Right*) Amplitude spectrum by ^{241}Am
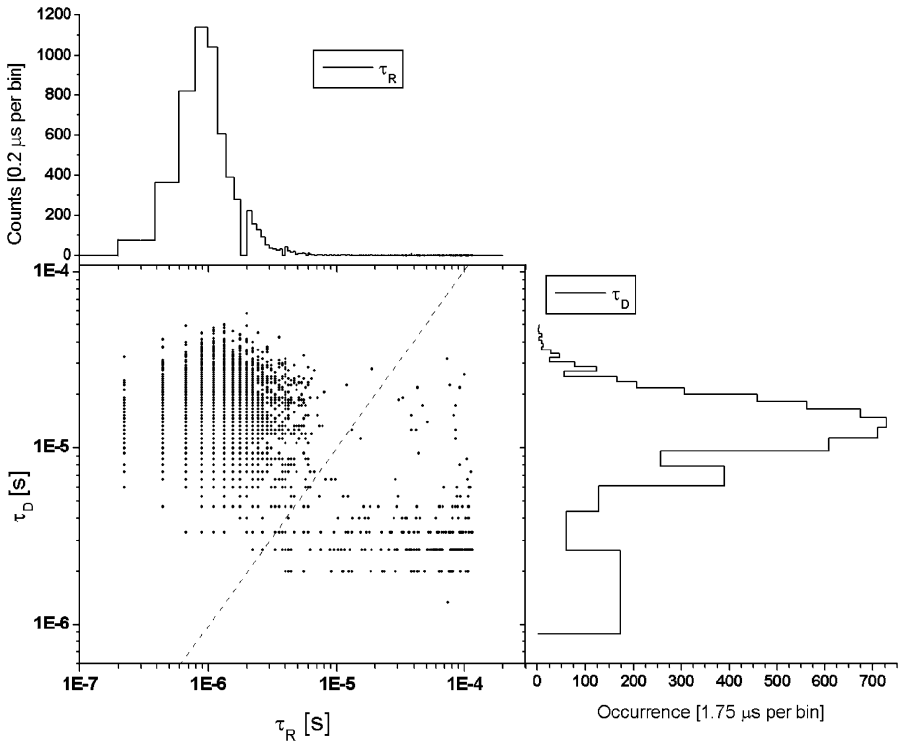

Fig. 7 AC-S2: PH vs Rise Time constant

Fig. 8 AC-S2: Decay Time constant vs Rise Time constant

is quite important to understand how the AC-S3 sample works, which is the next one.

About the Athermal-Thermal issue, we analyzed a set of well-shaped pulses well above the threshold where the signal-to-noise ratio is high. One pulse with overplotted the double pulse fit is shown in Fig. 10.

It is worth of note that also here, the decay time of the athermal component is close to the rise time of the thermal one, as expected.

As for AC-S1, the model shown in Fig. 1, provides for AC-S2 a thermal component compatible with the one shown in Fig. 10.

Indeed, if we see the spectrum shown in Fig. 6, its most part is constituted by pulses with a PH lower than the amplitude of the thermal component shown in Fig. 10, and they are especially related to the athermals: it is attributed to the detector. We do expect in our set up low energy component due to Cu fluorescence and Compton backscattering produced by 60 keV photons on the supporting structure. The expected count rate (verified also via GEANT4 simulations) should be few times larger than the count rate measured at 60 keV [6].

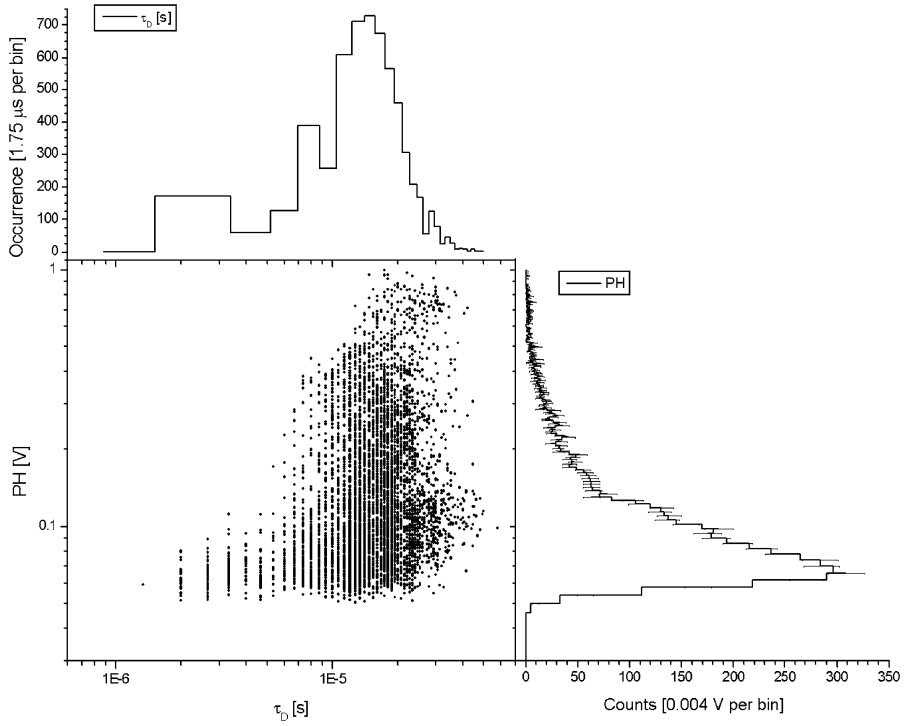Finally, the updated AC-S2 main results are summarized in Table 3.

Fig. 9 AC-S2: PH vs Decay Time constant

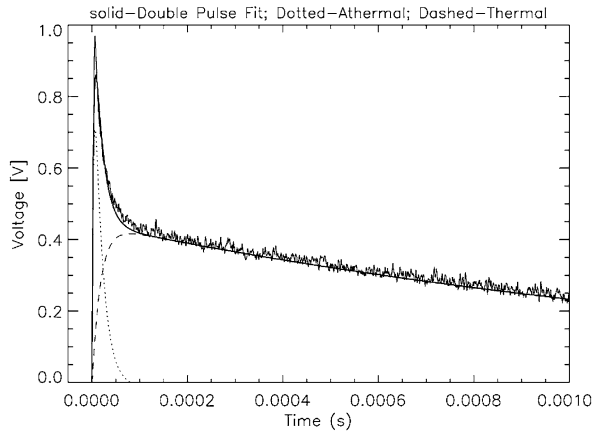**Fig. 10** AC-S2 pulse (high S/N ratio data) with double pulse fit

Table 3 Updated AC-S2 main results

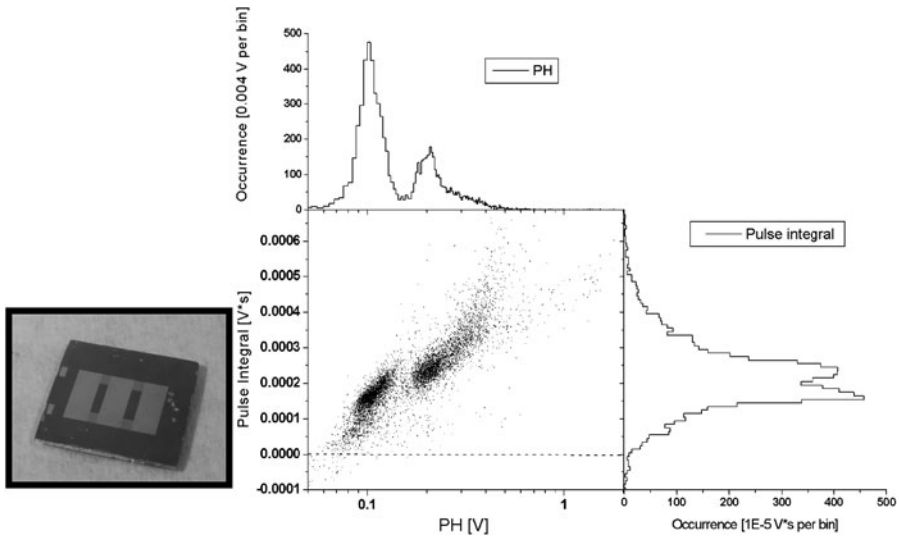| Collecting area (%)	τ_R [μs]	τ_D [μs]	Threshold [keV]	E_{max} [keV]
9	~1	15	40	7500

Fig. 11 (*Left*) The AC-S3 detector. (*Right*) Pulse integral vs PH analysis

4 AC-S3: Analysis and Results

In order to increase the collecting area for the phonons related to the athermal component we have increased the area of the Al pads. Figure 11 shows the AC-S3, which has been exposed only by the 60 keV of ^{241}Am.

Here the single Al pad has been increased up to 2×5 mm^2, more than 6 times the previous case. To better understand the spectrum, we performed an analysis both in PH and in integral modes. The result is shown in Fig. 11. It is evident the presence of two pulse families related to the double peak. The PH is correlated with the area: the greater the PH the greater the pulse integral. It is possible to disentangle this issue as shown in Fig. 12.

The different families are well featured by different rise time constants of about 40 μs and 300 μs: the greater the detected energy, the faster the pulse. The expected $\tau_R \sim 20$ μs, due to the L/R is consistent within a factor 2 with the fastest constant. The presence of a double peak is related to the diffusion of quasiparticles (qp) produced in Al (Fig. 13).

The Diffusion is $D = v_{\text{Fermi}} \cdot l_{\text{freepath}} = 1$ m^2/s (approx). Qp's should arrive in TES directly in μs in 1 mm path. In present Al film l_{freepath} resulted to be much lower than expected, probably due to impurities. Qp's diffuse slower and recombine before arriving in TES giving rise to phonons at the $2 \times$ gap energy. So, the most energetic peak is related to the phonons that directly couple to the TES, giving the fastest component. The conclusion is that it is necessary to improve Al film quality, and to tailor the size of Al absorber pad to maximize qp's collection in TES and minimize recombination. About the Decay Time Constant the plot is as for the one shown in [1], and due to the used filtering to reduce noise (bandwidth), we detect only the thermal component. There is a peak around 650 μs and no evidence of the two pulse families. The updated AC-S3 main results are summarized in Table 4.
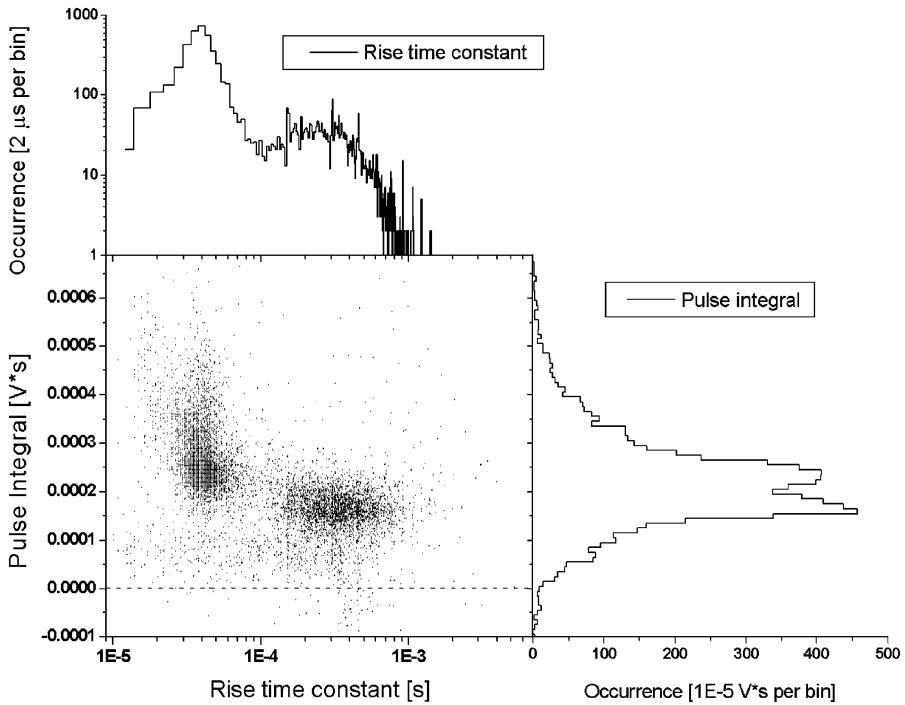
🖄 Springer

Fig. 12 Pulse integral vs Rise time constant

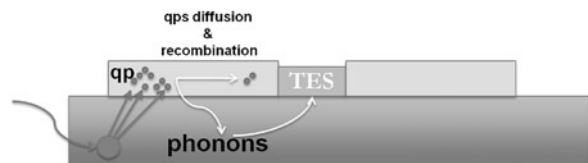**Fig. 13** Sketch of the dynamics to produce a double peak

Table 4 Updated AC-S3 main results

Collecting area (%)	τ_R (fast) [μs]	τ_D [μs]	Threshold keV	E_{max} keV
17	40	650	20	3100

5 AC-S4 and Further Improvements

We have under test a new prototype, AC-S4 similar to AC-S3, but with improved Al films (see Table 5 for the components size and Fig. 14 left).

AC-S4 is quite important also to get information about the Al-deposition. In parallel we are developing a prototype with 100 TES parallel and smaller Al fins, to minimize the travel time of QP in the collecting fins (Fig. 14-right). This detector will provide for fast response both to direct phonons and the quasi-particle "pulse" created in the phonon's collectors. The next Fig. 14 (right) shows the preliminary
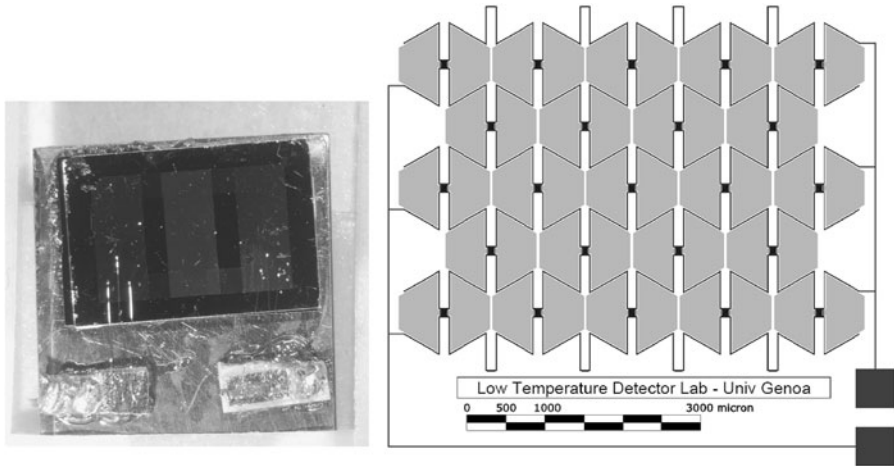
Fig. 14 (*Left*) AC-S4 sample. (*Right*) The future sample

Table 5 Components size for AC-S4

Silicon [mm^3]	Al-pads [thickness]	Ir-TES [area-thickness]	Collecting area (%)
$7 \times 10 \times 0.3$	230 nm	1×1.5 mm$^2 \times 135$ nm	$\sim$22

picture of a small square sector of the 18×18 mm future AC of 100 TES sensors (black) and phonon absorbers (light grey) borned for IXO but that will be scaled to ATHENA.

6 Conclusion

The results of the detailed analysis presented here confirm the solution adopted for the CryoAC of XMS, implementing the usage of fast athermal pulses and consolidate the scaling laws from small to large area.

The results from the first prototype (AC-S1) are within the requirements, with an area that is now just half of that required for the ATHENA baseline design which is based on 4 pixels.

The present family of large area ($\sim$1 cm^2) prototypes, with the new detector based on new Al pads under testing, originally developed for meeting the IXO design requirement, would therefore allow ample margins for the ATHENA design. For such detectors, there are still few open points that we are investigating.

References

1. C.K. Stahle et al., Proc. SPIE **3765**, 128 (1999)

2. C. Macculi et al., Proc. SPIE **7732**, 773 (2010)
3. F. Pröbst et al., J. Low Temp. Phys. **100**, 69 (1995)
4. S.H. Moseley, J.C. Mather, J. Appl. Phys. **56**, 1257 (1984)
5. M. Chapellier, Nucl. Instrum. Methods Phys. Res. A **520**, 21 (2004)
6. L. Piro et al., Report on the cryo-Anticoincidence detector for IXO-XMS, TN_ACD_10_1, Report to ESA for the IXO Technical Review (2010)
7. C. Macculi et al., in preparation
8. D. Cea, S. Lombardo, A. Ritacco, The astrophysics and the TES. Tech report of Astrophys. LAB for Degree in Phys., Univ. La Sapienza, Roma (2011)
9. M.R. Hauser et al., Phys. Rev. B **60**, 3072 (1999)
10. M.E. Msall, J.P. Wolfe, Phys. Rev. B **65**, 195205 (2002)